Transient Dynamics of Genetic Regulatory Networks

Matthew R. Bennett,*† Dmitri Volfson,*† Lev Tsimring,* and Jeff Hasty*†
*Institute for Nonlinear Science and †Department of Bioengineering University of California at San Diego, La Jolla, California

ABSTRACT We present an approximation scheme for deriving reaction rate equations of genetic regulatory networks. This scheme predicts the timescales of transient dynamics of such networks more accurately than does standard quasi-steady state analysis by introducing prefactors to the ODEs that govern the dynamics of the protein concentrations. These prefactors render the ODE systems slower than their quasi-steady state approximation counterparts. We introduce the method by examining a positive feedback gene regulatory network, and show how the transient dynamics of this network are more accurately modeled when the prefactor is included. Next, we examine the repressilator, a genetic oscillator, and show that the period, amplitude, and bifurcation diagram defining the onset of the oscillations are better estimated by the prefactor method. Finally, we examine the consequences of the method to the dynamics of reduced models of the phage lambda switch, and show that the switching times between the two states is slowed by the presence of the prefactor that arises from protein multimerization and DNA binding.

INTRODUCTION

As the complexity of gene regulatory networks under study increases so does the need for accurate modeling techniques (1). While exact numerical simulations are possible using Monte Carlo techniques like the Gillespie algorithm (2), such simulations can be computationally intensive. Continuous approximation schemes based on the underlying stoichiometric reactions can be used to simulate the dynamics of the average of each species in the system, but the complexity of these models can hinder both computational and theoretical analysis. Hence, many theorists have resorted to using a quasi-steady-state approximation (QSSA) (3,4) to reduce the number of dimensions in continuous models. Such reduced models do an excellent job in many cases, especially when the asymptotic state of the system is a stable equilibrium point. However, it has long been known that in some cases the QSSA does a poor job predicting the timescales over which systems equilibrate to their steady-state value (5–7). Moreover, interest is continually growing in gene networks that exhibit more complicated behavior, like stable limit cycles (8–11). When periodic behavior is present in a system, correct prediction of the timescales involved becomes necessary for a complete understanding of the system, and is essential for guiding experimental studies.

In this article, we present a continuous approximation scheme that reduces the number of dimensions in the system, while at the same time predicts the timescales of the full system more accurately than does the classic QSSA. By correctly applying multiple timescale analysis, the resulting reduced systems are the same as QSS approximations, but with a prefactor in front of the time derivatives of the concentrations. This method was first introduced by Kepler and Elston (6), and Bundschuh et al. (12) showed that the prefactor derived by Kepler and Elston was related to the Jacobian of a transformation relating monomer concentrations to the total concentration of a particular protein. We will examine this method in more detail, and demonstrate that the prefactors appear generally as a result of correct reduction of multiscale dynamics to a slow manifold in which fast dynamics are assumed to be in a local quasi-equilibrium.

We first introduce the approximation scheme by examining a simple example—the genetic feedback loop. We show that while both the prefactor method and the QSSA correctly predict the asymptotic behavior of the system, the transient dynamics are better modeled when the prefactor is included. Next, we look at a system with a stable limit cycle—the repressilator (8). While the QSSA correctly predicts oscillations in this system, we show that it incorrectly predicts the amplitude and frequency of those oscillations, which are better estimated with the new technique. Furthermore, the bifurcation between stable fixed points and limit cycles is more accurately estimated with the new scheme. In the last section, we will look at the lysis-lysogeny switch of bacteriophage λ. The temporal dynamics of the switch are an important aspect of its function, because the speed with which it makes transitions between the stable states will act as a limiting factor on the timescales at which the lytic cycle may be controlled. Therefore, reduced models describing the dynamics of the phage λ switch (or any switch) must accurately reproduce these timescales.

Timescale analysis of a genetic positive feedback loop

Separation of timescales is very common in the dynamics of gene regulatory networks. Many processes, like dimer- and tetramerization, occur at a much faster rate than other processes, such as transcription, translation, and degradation (4,13). Because the fast reactions are quick to equilibrate, it

Submitted August 21, 2006, and accepted for publication February 5, 2007.
Address reprint requests to J. Hasty, E-mail: hasty@bioeng.ucsd.edu.

0006-3495/07/05/3501/12 $2.00
doi: 10.1529/biophysj.106.095638

has been a common practice by many theorists to use a quasi-steady-state approximation to replace dynamical variables involved in these reactions with their steady-state values. This approximation reduces the number of dimensions in the resulting systems of ODEs, and hence greatly simplifies ensuing analysis.

Consider, for instance, the genetic positive feedback loop (4,14). This system involves a single gene that transcribes a single protein. Upon dimerization, the protein dimer can bind to an upstream regulatory site and stimulate transcription. Additionally, the protein monomer and the mRNA produced in transcription are subject to degradation. This situation is depicted in Fig. 1.

In this system there are nine reactions occurring among five chemical species. A list of these reactions is given in Table 1. Here x and y are the concentrations of protein monomers and dimers, respectively; d_0 is the concentration of promoter sites that are free of the dimer; d_r is the concentration of promoter sites that are bound to the protein dimer; and m is the concentration of mRNA strands.

The first four reactions in Table 1 represent the dimerization of the protein, the binding of the dimer to the upstream regulatory site, and their reverse processes. Reactions 5–7 represent transcription and translation, while the last two reactions are the degradation of the protein monomers and the mRNA. Reactions 1–4 typically occur at a much faster timescale than reactions 5–9.

From the reactions given in Table 1, we can write down a system of differential equations that represent the time evolution of the average concentration of each species. These equations are

$$\dot{x} = 2\kappa_- y - 2\kappa_+ x^2 + \sigma m - \gamma_p x \tag{1}$$

$$\dot{y} = \kappa_+ x^2 - \kappa_- y + k_- d_r - k_+ d_0 y \tag{2}$$

$$\dot{d}_0 = k_- d_r - k_+ y d_0 \tag{3}$$

$$\dot{d}_r = k_+ y d_0 - k_- d_r \tag{4}$$

$$\dot{m} = \alpha d_0 + \beta d_r - \gamma_m m, \tag{5}$$

where $\kappa_\pm$ and $k_\pm$ are the binding and dissociation rates of the proteins to themselves and the promoter site, respectively; γ_p and γ_m are the degradation rates of the protein monomers and mRNA, respectively; σ is the rate of translation; and α and β are the transcription rates from DNA with unbound and bound promoter sites, respectively. Equations 1–5 represent a complete description (in the thermodynamic limit) of the reactions given in Table 1. However, because the system is five-dimensional (and nonlinear), analysis is difficult. To get around this, previous studies have taken advantage of the differences in timescales. Recall that the dimerization and regulatory binding processes are fast compared to translation, transcription, and degradation. Equations 2–4 are dependent only on these reactions, and so will come to equilibrium faster than their slower counterparts, Eqs. 1 and 5. If we set the left-hand sides of Eqs. 2–4 equal to zero, and define $d = d_0 + d_r$ (here, d is the constant concentration of the gene), then we can solve for the steady-state values of y, d_0, and d_r in terms of x, with result

$$y = c_p x^2 \tag{6}$$

$$d_0 = d(1 + c_p c_d x^2)^{-1} \tag{7}$$

$$d_r = d c_p c_d x^2 (1 + c_p c_d x^2)^{-1}, \tag{8}$$

where $c_p = \kappa_+/\kappa_-$ and $c_d = k_+/k_-$. These steady-state values can now be placed into the ''slow'' equations, Eqs. 1 and 5, giving us the reduced system

$$\dot{x} = \sigma m - \gamma_p x \tag{9}$$

$$\dot{m} = \frac{d}{1 + c_p c_d x^2}[\alpha + \beta c_p c_d x^2] - \gamma_m m. \tag{10}$$

While Eqs. 9 and 10 correctly predict the steady-state asymptotics of the system, they do a poor job in predicting the transient dynamics of the system.

The problem with this method of reduction is in treating x as a slow variable. It is true that $\dot{x}$ depends on slow reactions (namely translation and degradation), but it also depends on two fast reactions (dimerization and dissociation). Therefore, x is not a slow variable, but a mixture of both slow and fast. While rigorous multiple timescale analysis is possible for systems such as these, it is not always necessary. In many cases, the variables can be transformed into ''slow'' and ''fast'' variables, so that the differential equations for the transformed variables contain either slow or fast reaction terms, but not both. Note that this does not imply that there are only two

TABLE 1 Reactions in the genetic positive feedback network

Number	Reaction		
1	$x + x$	$\xrightarrow{\kappa_+}$	y
2	y	$\xrightarrow{\kappa_-}$	$x + x$
3	$y + d_0$	$\xrightarrow{\kappa_+}$	d_r
4	d_r	$\xrightarrow{\kappa_-}$	$y + d_0$
5	d_0	$\xrightarrow{\alpha}$	$d_0 + m$
6	d_r	$\xrightarrow{\beta}$	$d_r + m$
7	m	$\xrightarrow{\sigma}$	$m + x$
8	x	$\xrightarrow{\gamma_p}$	Ø
9	m	$\xrightarrow{\gamma_m}$	Ø

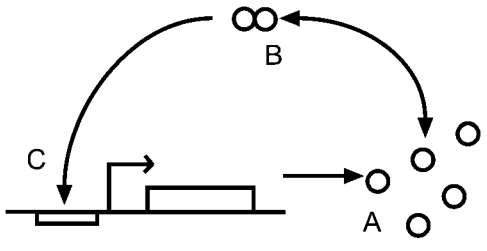

FIGURE 1 A schematic of the genetic positive feedback loop. The protein monomers (*A*) bind into dimers (*B*) that subsequently bind to the upstream regulatory site (*C*), activating production of the monomer.

timescales in the problem, since there are typically many timescales involved in such networks. Instead, by ''slow'' and ''fast'' we mean a partitioning of all timescales into two sets that are separated by at least an order of magnitude. When this occurs, the classic QSSA can be applied to the transformed system. Afterwards, the system must be transformed back into the original variables. For systems in which suitable transformations are not forthcoming, we provide in the Appendix a rigorous reduction scheme for a class of gene networks.

For the positive feedback loop in question, we can make the proper transformation by noting that both dimerization and dissociation keep the total number of protein molecules constant, while translation and degradation do not. Therefore, we can track the truly slow variable $n_x = x + 2y + 2d_r$, representing the total concentration of protein molecules (in any form), and write

$$\dot{n}_x = \sigma m - \gamma_p x. \tag{11}$$

The dynamical equation for x can be obtained from the transformation

$$n_x \approx x + 2c_p x^2 + 2c_p c_d d\frac{x^2}{1 + c_p c_d x^2}, \tag{12}$$

and therefore

$$\dot{n}_x = \dot{x}\frac{\partial n_x}{\partial x} = \dot{x}p(x), \tag{13}$$

where

$$p(x) = 1 + 4c_p x + \frac{4c_p c_d dx}{(1 + c_p c_d x^2)^2}. \tag{14}$$

Combining Eq. 11 with Eq. 14, we arrive at a new system of equations for the time evolution of x and m, namely,

$$p(x)\dot{x} = \sigma m - \gamma_p x, \tag{15}$$

$$\dot{m} = \frac{d}{1 + c_p c_d x^2}[\alpha + \beta c_p c_d x^2] - \gamma_m m. \tag{16}$$

Because $p(x)$ is a prefactor to the time derivative of x, any fixed point of the previous system (Eqs. 9 and 10) will also be a fixed point of the corrected system (Eqs. 15 and 16). Additionally, Eq. 14 implies $p(x) \geq 1$ when x is nonnegative, meaning that if both systems are attracted to the same fixed point the corrected system will necessarily relax to the fixed point slower than the old system—a fact noted by Pirone and Elston (15), when they examined the consequences of the prefactor to models of constitutively produced proteins.

Fig. 2 shows the dynamics of the protein monomer number in both the QSSA (*dashed curve*) and corrected version with the prefactor (*dash-dot curve*). Also shown is the result of integrating the full system, without any dimensional reduction (*solid curve*). The reduced system with the prefactor does a much better job in predicting the correct

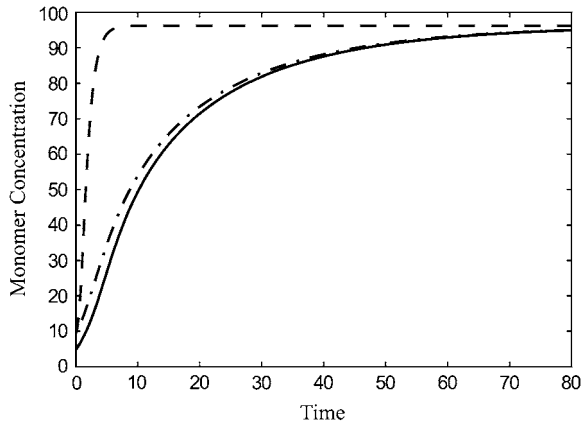

FIGURE 2 A comparison between the QSSA (*dashed curve*) and the ODE system with the prefactor correction (*dash-dot curve*) for a positive feedback gene network. Also shown (*solid curve*) is the nonreduced system of ODEs, Eqs. 1–5. Here $\kappa_+ = k_+ = 50$, $\kappa_- = k_- = 1000$, $\alpha = 1$, $\beta = 10$, $\sigma = 3$, $\gamma_p = 1$, $\gamma_m = 6$, and $n_c = 20$. The initial conditions are $x(0) = 10$, $x_2(0) = 0$, $m(0) = 0$, and $d_0(0) = d$.

timescale over which the system relaxes to the fixed point. Furthermore, the prefactor method estimates the relaxation time of the positive feedback loop throughout a wider range of parameter values more accurately than does the QSSA. Let $t_{1/2}$ be the time it takes the system to go from a zero concentration of proteins and mRNAs to the time at which the monomer concentration comes to one-half its steady-state value. Fig. 3 shows a comparison of the values of $t_{1/2}$ for the QSSA (*dashed curve*), prefactor method (*solid curve*), and the nonreduced system (*circles*) for a range of monomer degradation rates, γ_p. The prefactor method predicts $t_{1/2}$ more accurately than does the QSSA. Note that $t_{1/2}$ is not a monotonic function of the degradation rate. This is

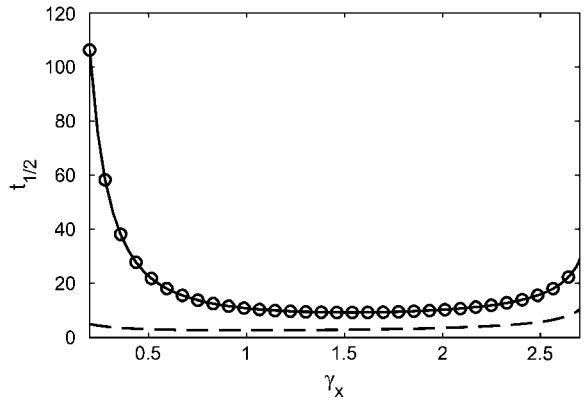

FIGURE 3 The relaxation times ($t_{1/2}$) as a function of γ_p for the QSSA (*dashed curve*), prefactor method (*solid curve*), and the nonreduced system (*circles*). Note that the values of $t_{1/2}$ predicted by the prefactor method are nearly identical with the true values obtained from the nonreduced system. Here $\kappa_+ = k_+ = 50$, $\kappa_- = k_- = 1000$, $\alpha = 1$, $\beta = 10$, $\sigma = 3$, $\gamma_m = 6$, and $d = 20$. The initial conditions are $x(0) = 0$, $x_2(0) = 0$, $m(0) = 0$, and $d_0(0) = d$.

due to our definition of $t_{1/2}$, and the existence of nonlinear positive feedback in the system. As the degradation rate is changed, so too is the position of the closest stable fixed point relative to our choice of initial conditions. Furthermore, because the relaxation is nonlinear, a true ''half-life'' for the relaxation can only be obtained very near the fixed points, making alternative measures of the relaxation necessary.

The repressilator

The correct estimation of the transient dynamics of genetic feedback loops may be of little consequence, since in most cases we are only concerned with the final state of the system. However, for such systems as oscillators, the final state will not be a stable fixed point. If accurate estimation of the timescales of the oscillations (i.e., periods) is desired, we cannot use the QSSA, since it incorrectly predicts these. To examine this issue, let us do another example, that of the repressilator system (8,16), as shown in Fig. 4. The repressilator is a three-element gene network based on a ring architecture in which each of the elements represses the next one down the line. In other words, gene G_1 (after transcription and translation of the resulting mRNA) produces protein x_1, which upon dimerization inhibits transcription of gene G_2. Similarly, the protein dimer y_2 represses the gene G_3, whose protein product, y_3, represses transcription of G_1.

The reactions of the repressilator are shown in Table 2. The first two equations represent the dimerization and dissociation of the protein monomers (x_i) and dimers (y_i). Reactions 3 and 4 are the binding and dissociation of the protein dimers to/from the free ($d_{0,i}$) and repressed ($d_{r,i}$) promoter sites. If the promoter of gene G_i is free (unrepressed) it can transcribe its associated mRNA (m_i), which in turn can translate its associated protein (reactions 5 and 6). Furthermore, the protein monomers and mRNAs will degrade with time (reactions 7 and 8).

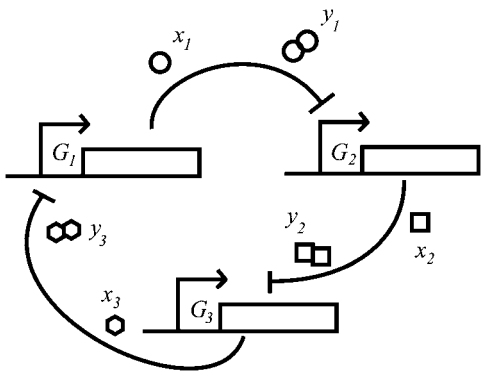

FIGURE 4 A schematic of the repressilator system. Gene G_1 produces protein x_1, which upon dimerization inhibits transcription of gene G_2. Similarly, the protein dimer y_2 represses the gene G_3, whose protein product, y_3, represses transcription of G_1.

TABLE 2 Reactions in the repressilator; here $i \in \{1, 2, 3\}$ while $k \in \{3, 1, 2\}$

Number	Reaction		
1	$x_i + x_i$	$\xrightarrow{\kappa_+}$	y_i
2	y_i	$\xrightarrow{\kappa_-}$	$x_i + x_i$
3	$d_{0,i} + y_k$	$\xrightarrow{k_+}$	$d_{r,i}$
4	$d_{r,i}$	$\xrightarrow{k_-}$	$d_{0,i} + y_k$
5	$d_{0,i}$	$\xrightarrow{\alpha}$	$d_{0,i} + m_i$
6	m_i	$\xrightarrow{\sigma}$	$m_i + x_i$
7	x_i	$\xrightarrow{\gamma_p}$	Ø
8	m_i	$\xrightarrow{\gamma_m}$	Ø

As before, we can use the reactions given in Table 2 to write a system of ODEs that represent the average concentrations of each species in the thermodynamic limit. These equations are

$$\dot{x}_i = -2\kappa_+ x_i^2 + 2\kappa_- y_i + \sigma m_i - \gamma_p x_i \tag{17}$$

$$\dot{y}_i = \kappa_+ x_i^2 - \kappa_- y_i - k_+ y_i d_{0,j} + k_- d_{r,j} \tag{18}$$

$$\dot{d}_{0,i} = -k_+ y_k d_{0,i} + k_- d_{r,i} \tag{19}$$

$$\dot{d}_{r,i} = k_+ y_k d_{0,i} - k_- d_{r,i} \tag{20}$$

$$\dot{m}_i = \alpha d_{0,i} - \gamma_m m_i, \tag{21}$$

where $i \in \{1, 2, 3\}$, $j \in \{2, 3, 1\}$, and $k \in \{3, 1, 2\}$.

As with the feedback system, we assume that dimerization and dissociation of the proteins (to themselves and the promoters) are fast compared to the other processes. If we take these reactions to be in equilibrium, we find that

$$y_i = c_p x_i^2 \tag{22}$$

and

$$d_{0,i} = d\{1 + c_d c_p x_k^2\}^{-1}, \tag{23}$$

where $d = d_{0,i} + d_{r,i}$ is the same constant concentration of each gene, $c_p = \kappa_+/\kappa_-$ and $c_d = k_+/k_-$. Since all the terms in Eq. 21 are slow, we can plug Eq. 23 into it to get

$$\dot{m}_i = \frac{\alpha d}{1 + c_d c_p x_k^2} - \gamma_m m_i. \tag{24}$$

Also, the total concentration of each protein is well approximated by

$$n_i = x_i + 2y_i + 2d_{r,j}, \tag{25}$$

$$\approx x_i + 2c_p x_i^2 + 2c_d c_p d x_i^2\{1 + c_d c_p x_i^2\}^{-1}. \tag{26}$$

The dynamics of n_i are governed by translation and monomer degradation, giving us

$$\dot{n}_i = \sigma m_i - \gamma_p x_i. \tag{27}$$

Using Eq. 25, we can write

$$\dot{n}_i = \dot{x}_i \frac{\partial n_i}{\partial x_i} = \dot{x}_i p(x_i), \tag{28}$$

where

$$p(x_i) = 1 + 4c_p x_i + \frac{4c_d c_p d x_i}{(1 + c_d c_p x_i^2)^2}. \quad (29)$$

If we use the rescalings $\gamma_m t \rightarrow t$, $\sqrt{c_d c_p}x_i \rightarrow x_i$, and $(\sigma\sqrt{c_d c_p})/(\gamma_m \beta)m_i \rightarrow m_i$, then we obtain the system

$$p(x_i)\dot{x}_i = -\beta(x_i - m_i), \quad (30)$$

$$\dot{m}_i = \frac{\kappa d'}{1 + x_k^2} - m_i, \quad (31)$$

where $\beta = \gamma_p/\gamma_m$, $\kappa = \alpha\sigma/\gamma_m\gamma_p$, $d' = \sqrt{c_d c_p}d$ and the overdot now represents differentiation with respect to the rescaled time. When suitably rescaled, the prefactor reads

$$p(x_i) = 1 + 4rx_i + \frac{4d' x_i}{(1 + x_i^2)^2}, \quad (32)$$

where $r = \sqrt{c_p/c_d}$. Qualitatively, the parameter r is related to the equilibrium ratios of dimers to monomers and unbound to bound promoter sites. If the ratio of unbound to bound promoter sites is near unity, then r is of the order of the ratio of dimers to monomers. Specifically,

$$r = \frac{\bar{y}}{\bar{x}}\sqrt{\frac{\bar{d}_0}{\bar{d}_r}}, \quad (33)$$

where the overbar represents quasi-equilibrium values, and the indices are suppressed due to symmetry.

When the prefactor, $p(x_i)$, is set to unity, Eqs. 30 and 31 are exactly the equations produced by the QSSA for the repressilator system (8). Both sets of equations still have regions of stable limit cycles, but the prefactor version more accurately reproduces the full dynamics of the system. This can be seen in Fig. 5. Fig. 5 *a* shows the results of a simulation of the full, unreduced equations, Eqs. 34–37, while Fig. 5, *b* and *c*, are from the QSSA and the prefactor method, respectively. Notice that the prefactor method does a much better job in estimating both the period and the amplitude of the oscillations. This can also be seen in Fig. 6, *a* and *b*, which show the period and amplitude of each of the three systems as a function of γ_p.

To guide experiments, it is necessary to estimate the regions in parameter space where one should expect stable limit cycles. The prefactor, Eq. 32, contains the parameter r which does not appear in the QSSA and as the value of r is changed (which amounts to changing the ratio of c_d to c_p while keeping their product fixed), the bifurcation curve separating stable fixed points from stable limit cycles (in κ–β space) changes. This is shown in Fig. 7 *a*. The solid line represents the bifurcation between stable fixed points (to the *left* of the *curve*) and stable limit cycles (to the *right* of the

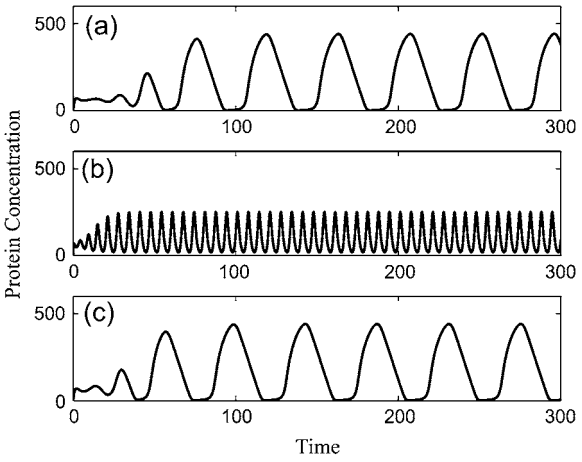

FIGURE 5 An example of the oscillations seen in the repressilator system for (*a*) the unreduced equations, Eqs. 34–37, (*b*) the QSSA—i.e., Eqs. 30 and 31 with $p(x_i) = 1$, and (*c*) the prefactor method approximation, Eqs. 30 and 31. Here $\gamma_p = 6$, $\gamma_m = 1$, $\kappa_+ = k_+ = 5$, $\kappa_- = k_- = 100$, $\alpha = 10$, $\sigma = 20$, and $d = 20$. The initial conditions were $x_i = 10$, $y_i = 0$, $d_i = d$, and $m_i = 0$.

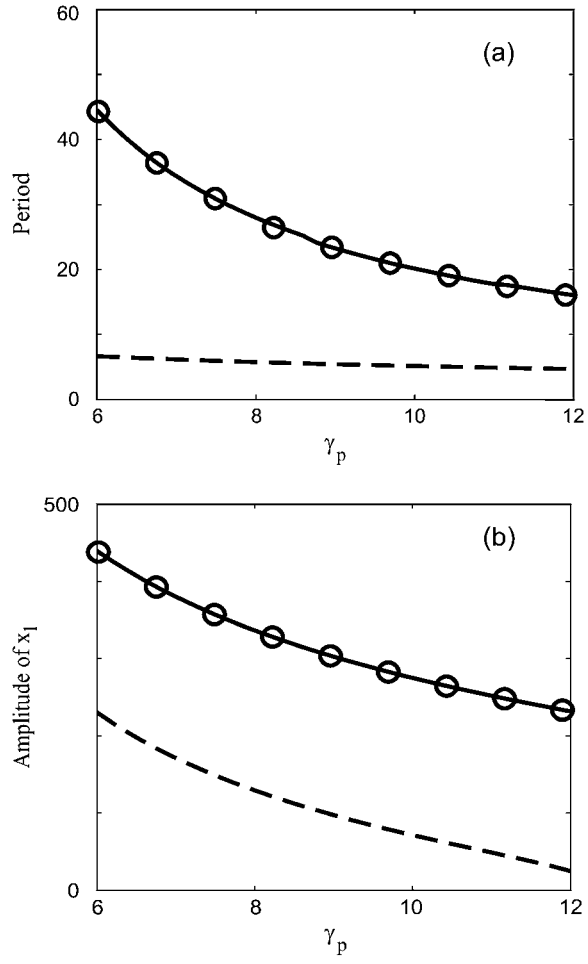

FIGURE 6 A comparison of the period (*a*) and amplitude (*b*) of the oscillations as a function of the protein degradation rate in the repressilator for the unreduced equations (*black curves*), the prefactor method (*circles*), and the QSSA (*dashed curves*). Here, we calculate the amplitude by $\max(x_1) - \min(x_1)$ on the limit cycle. The parameters for these figures are the same as those in Fig. 5.

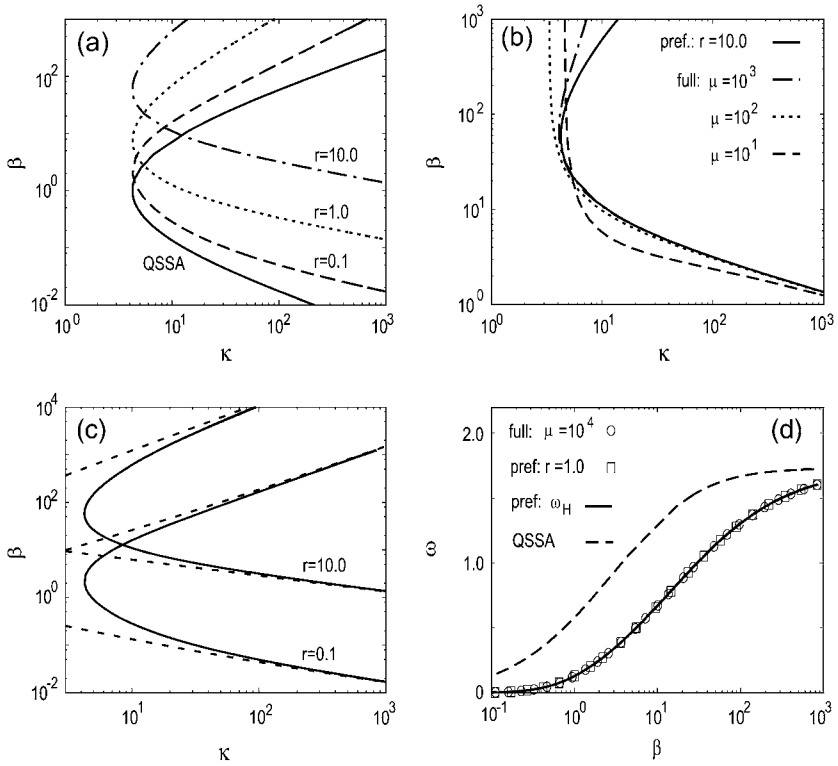

FIGURE 7 Comparison of the parameter space for each model. (*a*) Bifurcation diagram for the repressilator. The solid line represents the bifurcation curve of the QSSA between stable fixed points (to the *left* of the *curve*) and stable limit cycles (to the *right* of the *curve*). The remaining curves are the same bifurcation curves for the prefactor method with $r = 10$ (*dash-dot*), $r = 1$ (*dotted*), and $r = 0.1$ (*dashed*). For each of the prefactor curves the parameters are such that, while r differs, the corresponding parameters for the QSSA are the same. The curves for the full system virtually coincide with the curves for prefactor model ($\mu = \nu = 10^4$) and are not shown for clarity. For all curves, $d' = 1$. (*b*) Comparison of the Hopf curves for the prefactor model with the results for the full system for different values of $\mu = \nu$. The difference becomes significant as μ and ν are decreased and the assumption of the separation of timescales breaks down. All curves are for $r = 10$ and $d' = 1$. For smaller values of r and/or d', the instability threshold predicted with the prefactor model converges to the threshold for the full system at smaller values of μ (not shown). (*c*) Comparison of the Hopf curves for the prefactor model computed numerically for $r = 0.1$ and $r = 10$ (for $d' = 1$, *solid lines*) with the asymptotic approximations (*dashed lines*), Eqs. 39 and 42. (*d*) The frequency of the unstable mode along the threshold as a function of β. Circles and squares correspond to numerical results for the full system ($\mu = \nu = 10^4$) and for the prefactor method, respectively. The solid line corresponds to the function ω_H specified by Eq. 43. The dashed line predicted by QSSA systematically overestimates the frequency of the oscillatory instability. All curves are for $r = 1$ and $d' = 1$.

curve) according to the QSSA. As long as the product $c_d c_p$ remains fixed, the bifurcation curve will not change, no matter what the ratio is. This is in contrast to the predictions of the prefactor method. While keeping all the parameters the same as in the QSSA, we change the parameter r to see how the bifurcation curve changes. The colored curves in Fig. 7 *a* represent the bifurcation curve for $r = 10$ (*dash-dot*), $r = 1$ (*dotted*), and $r = 0.1$ (*dashed*). As $r \to 0$, the prefactor approximation approaches the QSSA, and as r increases, there is a significant divergence between the regions in parameter space in which stable limit cycles are present for the two methods. Because the timescales of the full system are more accurately predicted with the prefactor method, it does a better job in estimating the region of oscillations than does the QSSA.

To compare these results with the full model, we rescale the additional variables that do not appear in the reduced systems. If we use the same rescalings as before, the dimensionless form the full system for repressilator becomes

$$\dot{x}_i = -2\mu(x_i^2 - y_i) + \beta(m_i - x_i) \tag{34}$$

$$\dot{y}_i = \mu(x_i^2 - y_i)r^{-1} - \nu r^{-2}(y_i d_{0,j} + d_{0,j} - d') \tag{35}$$

$$\dot{d}_{0,i} = -\nu r^{-1}(y_k d_{0,i} + d_{0,i} - d') \tag{36}$$

$$\dot{m}_i = \kappa d_i - m_i, \tag{37}$$

where we have used the additional rescalings $c_d y_i \to y_i$, $d_{0,i}\sqrt{c_d c_p} \to d_{0,i}$, and we have introduced the new parameters $\nu = k_-/\gamma_m$, $\mu = \kappa_-/\gamma_m$. When μ and ν are sufficiently large, we expect the properly reduced system (with prefactors) to faithfully reproduce the dynamics of the full system. We find that when $\mu = \nu \gtrsim 10^4$ (corresponding to dissociation rates that are much larger than the mRNA degradation rate), the prefactor method accurately predicts the bifurcation boundary. As $\mu = \nu$ decreases, the shape of the boundary changes in a nontrivial way, as shown in Fig. 7 *b*. Here the solid line represents the prediction of the prefactor method for $r = 10$. Also shown are three boundaries of the full system for several different values of $\mu = \nu$.

When $\mu = \nu$ is large enough, it becomes possible to predict the onset of the instability leading to the limit cycle. The system of equations, Eqs. 30 and 31, always has a symmetric equilibrium $S = (x_i, m_i) = (\bar{x}, \bar{x})$ parameterized by $\bar{x} = \bar{x}(\kappa d')$, which is the unique real solution of the equation

$$\bar{x} + \bar{x}^3 = \kappa d'. \tag{38}$$

Bifurcation analysis of this steady state reveals that S becomes unstable through a supercritical Hopf bifurcation, thus giving rise to a stable limit cycle. The threshold of the instability and the frequency ω_H of an unstable mode may be found from the characteristic equation, which is a sixth-order

polynomial for the eigenvalue $\lambda = i\omega_H$. A neutral surface $F(\beta, \kappa d', \bar{x}, r) = 0$ may be found in a closed form; however, it is more instructive to consider particular limits when $\kappa d' \gg 1$ and either $\beta \gg 1$ or $\beta \ll 1$. Keeping only leading-order contributions, we find

$$\beta \ll 1, \quad \beta \approx \frac{1}{3(\kappa d')^{2/3}} + \frac{4r}{3(\kappa d')^{1/3}}, \tag{39}$$

$$\beta \gg 1, \quad \beta \approx 3(\kappa d')^{2/3} + 12r\kappa d'. \tag{40}$$

In the case of the QSSA, the same distinguished limits are described by similar expressions,

$$\beta \ll 1, \quad \beta \approx \frac{1}{3(\kappa d')^{2/3}}, \tag{41}$$

$$\beta \gg 1, \quad \beta \approx 3(\kappa d')^{2/3}. \tag{42}$$

Notice that the boundaries for the prefactor method (Eqs. 39 and 40) both contain an extra term proportional to r that is not in the boundaries of the QSSA (Eqs. 41 and 42). These extra terms are responsible for the divergence of the prefactor method from the QSSA seen in Fig. 7 *a* as r increases from zero. Fig. 7 *c* shows the accuracy of the boundary estimates for the prefactor method for two values of $\mu = \nu$.

The Hopf frequency may be expressed in a compact form, for both the prefactor method and the QSSA, with result

$$\omega_H^2 = \frac{Q(B)}{6} - \frac{B+1}{6}\sqrt{Q(B) + 6B}, \tag{43}$$

where $Q(B) = B^2 + 8B + 1$ and $B = \beta/p(\bar{x})$. In the QSSA case $p(\bar{x}) = 1$, so $B = \beta$. Since ω_H is the monotonously increasing function of B (see Fig. 7 *d*) and $B \leq \beta$ we conclude that the prefactor method always predicts lower frequencies at the threshold; the difference with the QSSA method becomes more pronounced for larger values of $p(\bar{x})$ and therefore for larger r and/or d'.

The phage λ-switch

One important class of gene networks is the toggle switch (17). These networks are designed to respond to an external signal in such a way that they are either on (fully induced) or off (no transcription). A quantitative understanding of the dynamics of gene switches is a crucial first step toward a modular description of gene regulation. In addition, the ability to rapidly switch between multiple stable states is important to the development of sophisticated cellular control schemes. Nonlinearities giving rise to two stable states suggest the possibility of using these states as digital signals to be processed in cellular-level computations (18,19). One may eventually be able to produce systems in which sequences of such switching events are combined to control gene expression in complex ways. In any such application, the speed with which systems make transitions between their stable states will act as a limiting factor on the timescales at which cellular events may be controlled. With this in mind, it becomes important that mathematical models of gene switches correctly predict the timescales over which they travel from one state to the other.

The genetic network of λ-phage switches its host bacterium from the dormant lysogenous state to the lytic growth state in ~20 min (13,20). As shown in Fig. 8, it consists of two promoters, P_R and P_{RM}, which share three operator sites, O_R1, O_R2, and O_R3. The product of the left promoter (P_{RM}) is the protein cI, which (upon dimerization) can bind to the promoter sites. When cI is bound, its purpose is twofold. First, it activates transcription of the left promoter, causing a positive feedback loop. Second, it represses the right promoter (P_R), blocking its transcription. The system will remain in this state until some external signal (such as UV radiation) causes the rapid degradation of cI. This is done by an activated form of the protein RecA, which cleaves cI monomers, rendering them incapable of dimerizing. At this point, the concentration of cI becomes low enough to free up the promoter sites, releasing the P_R so that it may produce its protein, Cro. Cro can then bind to the promoter sites, repressing the production of cI.

Transcription of repressor (cI) takes place when there is no protein (of either type) bound to O_R3. When repressor is bound to O_R2, the rate of repressor transcription is enhanced, and Cro is transcribed only when O_R3 is either vacant, or has a Cro dimer bound to it. If either repressor or Cro is bound to either O_R1 or O_R2, the production of Cro is halted. For brevity, we omit the full derivation of the equations of motion, and ignore the intermediate step of mRNA translation. This step can easily be put into the model, but it will not affect the timescale analysis, or the prefactor. For a listing of the relevant chemical reactions in the phage λ-switch and a derivation of the equations without the prefactor, we refer the interested reader to Hasty et al. (4). Letting x and y represent the concentrations of cI and Cro, the competition for operator sites leads to deterministic rate equations of the form

$$(M_{xx} + M_{xy})\dot{x} = m(1 + x^2 + \alpha\sigma_1 x^4)/Q - \gamma_x x, \tag{44}$$

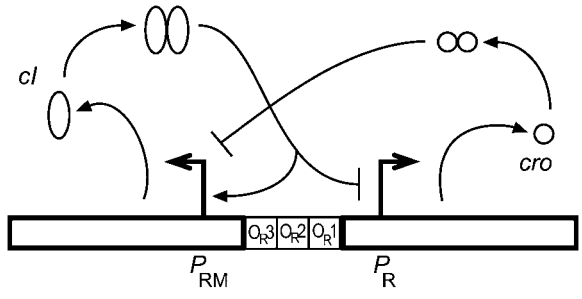

FIGURE 8 Genetic network diagram of the phage λ switch. The left promoter produces cI, which activates itself and represses the right promoter. The right promoter produces Cro, which represses the left promoter. Both of the proteins, cI and Cro, can bind to the three promoter sites once they have dimerized.

$$(M_{yx} + M_{yy})\dot{y} = m\rho_y(1 + y^2)/Q - \gamma_y y, \quad (45)$$

where the 2×2 matrix $\mathbf{M}$ and Q are given by

$$M_{ij} = \partial_j N_i, \quad i,j \in \{x,y\} \quad (46)$$

$$N_x = x + 2x^2[\sqrt{K_1/K_2} + m(1 + 3\sigma_2\sigma_1 x^4 + 2\sigma_1 x^2 + 2\sigma_1\beta_4 x^2 y^2 + \beta_5 y^2)/Q] \quad (47)$$

$$N_y = y + 2y^2[\sqrt{K_3/K_4} + m(1 + 3\beta_1\beta_3 y^4 + 2(\beta_1 + \beta_2)y^2 + \beta_5 x^2 + \beta_4\sigma_1 x^4)/Q] \quad (48)$$

$$Q = 1 + x^2 + \sigma_1 x^4 + \sigma_1\sigma_2 x^6 + y^2 + (\beta_1 + \beta_2)y^4 + \beta_1\beta_3 y^6 + \sigma_1\beta_4 x^4 y^2 + \beta_5 x^2 y^2, \quad (49)$$

where m is the plasmid copy number, and we have rescaled the concentrations by $x/\sqrt{K_1K_2} \to x$, and $y/\sqrt{K_3K_4} \to y$. The equilibrium constants K_i are for cI dimerization and cI-O_R1 binding (K_1 and K_2), and for cro dimerization and Cro-O_R3 binding (K_3 and K_4), and the σ_i and β_i parameters describe the relative probabilities for cI (σ_i) and cro (β_i) binding configurations to O_R1, O_R2, and O_R3. In the above equations, the right-hand sides of Eqs. 44 and 45 describe the slow reactions responsible for the changes in the total numbers of proteins, and the Jacobian matrix $\mathbf{M}$ is made of partial derivatives of $N_{x,y}$ with respect to (x, y). N_x and N_y represent the total concentrations of cI and Cro, taking into account the monomeric, dimeric, and promoter site-bound dimer forms of each protein. Because the dynamics of N_x and N_y are affected only by the slow reactions of transcription and degradation, they are computed under the assumption that the fast reactions reach equilibrium. The matrix terms that form the prefactors of Eqs. 44 and 45 describe the lumped influence of the dynamics of the fast reactions on the dynamics of slow reactions. When the prefactors are set to unity (i.e., $\mathbf{M} = \mathbf{I}$), Eqs. 44 and 45 represent the QSSA of this model.

Fig. 9 shows simulations of Eqs. 44 and 45, with and without the prefactor. Before irradiation with UV light, cI is in its high state, while the concentration of Cro is near zero. At time $t = 0$ the irradiation occurs, and the degradation rate of cI is increased. Subsequently, the concentration of cI becomes very low, while the concentration of Cro becomes very high, beginning the lytic process in phage λ. Notice that the timescales over which the switch changes states is much longer when the prefactor is included.

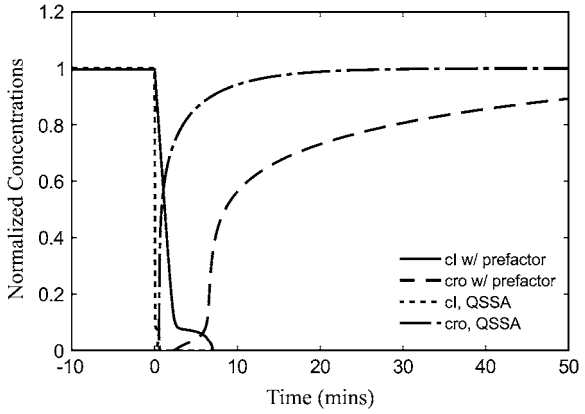

FIGURE 9 Dynamics of the phage λ switch. Here, the parameters are $m = 20$, $\alpha = 11$, $\rho_y = 62.92$, $\sigma_1 = 2$, $\sigma_2 = 0.8$, $\beta_1 = \beta_2 = \beta_3 = 0.08$, $\beta_4 = \beta_5 = 1$, $K_1 = K_3 = 5 \times 10^7$ M^{-1}, $K_2 = K_4 = 3.3 \times 10^8$ M^{-1}, and $\gamma_y = 0.03$ min^{-1}. For $t < 0$, $\gamma_x = 0.03$ min^{-1}. At time $t = 0$ the degradation rate of cI is increased to $\gamma_x = 30$ min^{-1}, representing cleavage of cI by the activated form of RecA due to an increase in UV radiation.

DISCUSSION

We have introduced a method for approximating and reducing the full systems of ODEs for genetic regulatory networks. Like the QSSA, the prefactor method simplifies the analysis of such systems by reducing the number of dimensions. Unlike the QSSA, however, the timescales of the system are preserved. Timescale problems have long been known to exist when using the QSSA to derive Michaelis-Menten type reaction equations for enzyme kinetics (21–24). It is not surprising, then, that timescale problems arise when using the QSSA to derive reduced equations for genetic regulatory networks.

The timescale problems can be overcome with the correct use of timescale separation. While we have shown that a rigorous approach can be derived, one based on multiple timescale analysis, we have also shown that one can derive prefactors by plugging the equilibrium values of the ''fast'' reactants into differential equations for the slow variables. Generally, the slow variables are not the protein concentrations, but instead are total concentrations of all versions of the specific protein (free or bound into dimers or larger complexes), since the total number of proteins in any form is affected only by the slow reactions of translation and degradation.

In general, the inclusion of the prefactors into the analysis slows down the resulting dynamics of the reduced system. Whereas standard QSSA generally has faster dynamics than the nonreduced system, the prefactor method estimates the timescales very accurately. This accuracy is of paramount importance when modeling gene networks designed to exhibit temporal dynamics (25). For instance, the time that it takes for a genetic switch (26,27) to move from one stable fixed point to another can have important consequences. Furthermore, when designing genetic oscillators, it becomes necessary to correctly predict the regions in parameter space in which oscillations are expected. As we saw with the repressilator, the prefactor method predicts these regions more accurately than does the QSSA. In many cases, the separation of timescales is the key to nontrivial behavior, and correctly modeling such systems is therefore necessary.

It should be noted that in this article we have ignored the stochastic fluctuations due to the intrinsic randomness of the

underlying biochemical reactions (2,6,28). These fluctuations can have profound effects on networks, and the timescales of their correlations may determine the nature of their influence (29). A procedure similar to the one given above that does include stochasticity involves the reduction of the full multidimensional master equation onto a manifold of slowly evolving variables (6,12). One can then derive corresponding Langevin equations for protein concentrations that will have similar prefactor terms to the ones derived here. However, these equations ignore the stochasticity inherent in the fast reactions. It is still an open question, then, how to project a full system of Langevin equations (containing both slow and fast reactions) onto a slow manifold while preserving the stochastic effects of the fast reactions. We are planning to address this issue in our future work.

APPENDIX: GENERAL METHOD OF TIMESCALE ANALYSIS FOR GENE NETWORKS

While the procedures given above for reducing systems of ODEs for gene regulatory networks are illustrative, a more rigorous approach may be desired. To this end, we present in this Appendix a method based on multiple timescale analysis (30) for projecting the full dynamics onto a slow manifold for a general regulatory network.

Let us consider a general framework for a genetic regulatory network. The notations for the components of the network are listed in Table A1. We assume that the network consists of N genes each with a concentration d_i ($i = 1, \ldots, N$). These genes transcribe N corresponding mRNAs, denoted by m_i. The mRNAs, in turn, are translated at a rate σ_i to produce n_i protein monomers, x_i. Each protein can form an associated dimer, y_i, with rates κ_i and κ_{-i} for dimerization and dissociation, respectively. Accompanying each gene is a promoter that may contain one or more binding sites to which the protein dimers may bind, and thereby enhance or diminish the transcription rate of the gene.

TABLE A1 Notation for the generalized genetic network model

Symbol	Description
d_i	Gene concentrations.
x_i	Monomer concentrations.
y_i	Dimer concentrations.
m_i	mRNA concentrations.
σ_i	Translation rates.
$\gamma_{p,i}$	Degradation rates of the monomers.
$\gamma_{m,i}$	Degradation rates of the mRNA.
p_{ij}	Rate at which protein i is degraded by protein j.
d^i_{j0}	Unoccupied binding site O^i_j.
$\mathbf{D}_i$	Matrix of occupied binding site concentrations for the i^{th} gene.
d^i_{jn}	The j^{th}, n^{th} element of $\mathbf{D}_i$ (binding site O^i_j occupied by protein n).
n_i	Number of protein molecules translated per one mRNA.
O^i_j	Label for the j^{th} binding site of the i^{th} gene.
N	Number of genes.
M_i	Number of binding sites of the i^{th} gene.
$\kappa_{\pm i}$	Dimerization/dissociation rates of the proteins to/from themselves.
α_i	Transcription rate of the i^{th} gene.
$\mathbf{K}_{\pm i}$	Rate matrix for the binding/dissociation of the dimers to the promoter sites.
$k^{\pm i}_{jn}$	The j^{th}, n^{th} element of $\mathbf{K}_{\pm i}$ (binding/dissociation rate of the n^{th} dimer to the j^{th} binding site of the i^{th} gene).
H_i	The ratio κ_i/κ_{-i}.
G^i_{jn}	The ratio k^i_{jn}/k^{-i}_{jn}.

We assume that the promoter for the i^{th} gene contains M_i binding sites O^i_j ($j = 1, \ldots, M_i$) and any protein can bind to any of the M_i binding sites of the i^{th} promoter. We denote by d^i_{j0} the concentration of unoccupied binding sites O^i_j, and by d^i_{jn} the concentration of the binding sites O^i_j occupied by n^{th} protein. Note that the sum

$$\sum_{n=0}^{N} d^i_{jn} = d_i \tag{A1}$$

is the constant concentration of the i^{th} gene. In what follows, if we refer to d^i_{jn} we will be referring to bound promoter sites ($n > 0$) unless we explicitly refer to d^i_{j0} or unless it is used in a sum such as $\sum_{n=0}^{N} d^i_{jn}$.

The transcription rate of the i^{th} gene is α_i, which is a function of the current state of the promoter (i.e., which regulatory proteins are bound to which promoter sites). In general, we can include this dependency by making the transcription rates functions of the bound promoter site concentrations, i.e., $\alpha_i = \alpha_i(\mathbf{D}_i)$, where $\mathbf{D}_i$ is an $M_i \times N$ matrix with elements d^i_{jn}. As written, $\alpha_i(\mathbf{D}_i)$ can be thought of as the transcriptional rate of the i^{th} gene, averaged over each copy of that gene. In other words, we can write

$$\alpha_i(\mathbf{D}_i) = \langle \alpha_i(\mathbf{s}_i) \rangle_{si}, \tag{A2}$$

where $\mathbf{s}_i = \{\nu_1, \nu_2, \ldots, \nu_{M_i}\}$ is an M_i-tuple of integers representing a possible configuration of a gene, consisting of protein ν_k occupying the k^{th} promoter site, and $\langle \ldots \rangle_{si}$ represents averaging over all $(N+1)^{M_i}$ possible states of the promoter. If $\nu_k = 0$, then that particular binding site is free. The binding/dissociation rates of the proteins to the i^{th} promoter are described by two $M_i \times N$ matrices, $\mathbf{K}_i$ and $\mathbf{K}_{-i}$, with components k^i_{jn} and k^{-i}_{jn}, respectively. We will assume that there is no cooperativity between the binding of the proteins to the promoter sites, so that $\mathbf{K}_{\pm i}$ is not a function of $\mathbf{D}_i$. This assumption is made to simplify the analysis, but is not necessary. We also include into the consideration protein-protein interactions: protein j may play a role of protease for the protein i, with p_{ij} denoting the corresponding degradation rate. Finally, both the protein monomers and the mRNA will degrade at rates $\gamma_{p,i}$ and $\gamma_{m,i}$, respectively. The chemical reactions occurring in the network are listed in Table A2.

From the reactions given in Table A2 we can write down a system of ODEs corresponding to the time evolution of the concentrations of each of the chemical species. As a result, we obtain

$$\dot{x}_i = -2\kappa_i x_i^2 + 2\kappa_{-i} y_i - \gamma_{p,i} x_i + \sigma_i n_i m_i - x_i \sum_{j=1}^{N} p_{ij} x_j \tag{A3}$$

$$\dot{y}_i = \kappa_i x_i^2 - \kappa_{-j} y_i + \sum_{n=1}^{N} \sum_{j=1}^{M_n} \left[-k^n_{ji} d^n_{j0} y_i + k^{-n}_{ji} d^n_{ji} \right] \tag{A4}$$

$$\dot{d}^i_{jn} = k^i_{jn} d^i_{j0} y_n - k^{-i}_{jn} d^i_{jn} \tag{A5}$$

TABLE A2 Reactions in the generalized genetic network model

Number	Reaction			Rate
1	$x_i + x_i$	$\xrightarrow{\kappa_i}$	y_i	$\kappa_i x_i^2$
2	y_i	$\xrightarrow{\kappa_{-i}}$	$y_i + y_i$	$\kappa_{-i} y_i$
3	x_i	$\xrightarrow{\gamma_{p,i}}$	$\emptyset$	$\gamma_{p,i} x_i$
4	$x_i + x_j$	$\xrightarrow{p_{ij}}$	x_j	$p_{ij} x_i x_j$
5	d_i	$\xrightarrow{\alpha_i}$	$d_i + m_i$	$\alpha_i(\mathbf{D}_i) d_i$
6	$d^i_{j0} + y_n$	$\xrightarrow{k^i_{jn}}$	d^i_{jn}	$k^i_{jn} d^i_{j0} y_n$
7	d^i_{jn}	$\xrightarrow{k^{-i}_{jn}}$	$d^i_{j0} + y_n$	$k^{-i}_{jn} d^i_{jn}$
8	m_i	$\xrightarrow{\sigma_i}$	$m_i + n_i x_i$	$\sigma_i m_i$
9	m_i	$\xrightarrow{\gamma_{m,i}}$	$\emptyset$	$\gamma_{m,i} m_i$

$$\dot{d}^{\mathrm{i}}_{\mathrm{j}0} = -\sum_{\mathrm{n}=1}^{\mathrm{N}} k^{\mathrm{i}}_{\mathrm{jn}} d^{\mathrm{i}}_{\mathrm{j}0}\, y_{\mathrm{n}} + \sum_{\mathrm{n}=1}^{\mathrm{N}} k^{-\mathrm{i}}_{\mathrm{jn}} d^{\mathrm{i}}_{\mathrm{jn}} \tag{A6}$$

$$\dot{m}_{\mathrm{i}} = d_{\mathrm{i}}\alpha_{\mathrm{i}}(\mathbf{D}_{\mathrm{i}}) - \gamma_{\mathrm{m,i}} m_{\mathrm{i}}. \tag{A7}$$

Because of conservation of the total concentration of the genes, Eq. A6 can be eliminated, and $d^{\mathrm{i}}_{\mathrm{j}0}$ replaced by $d_{\mathrm{i}} - \sum_{\mathrm{n}=1}^{\mathrm{N}} d^{\mathrm{i}}_{\mathrm{jn}}$, giving us

$$\dot{x}_{\mathrm{i}} = -2\kappa_{\mathrm{i}} x_{\mathrm{i}}^2 + 2\kappa_{-\mathrm{i}} y_{\mathrm{i}} - \gamma_{\mathrm{p,i}} x_{\mathrm{i}} + \sigma_{\mathrm{i}} n_{\mathrm{i}} m_{\mathrm{i}} - x_{\mathrm{i}} \sum_{\mathrm{j}=1}^{\mathrm{N}} p_{\mathrm{ij}} x_{\mathrm{j}} \tag{A8}$$

$$\dot{y}_{\mathrm{i}} = \kappa_{\mathrm{i}} x_{\mathrm{i}}^2 - \kappa_{-\mathrm{j}} y_{\mathrm{i}} + \sum_{\mathrm{n}=1}^{\mathrm{N}} \sum_{\mathrm{j}=1}^{\mathrm{M_n}} \left[-k^{\mathrm{n}}_{\mathrm{ji}} \left(d_{\mathrm{n}} - \sum_{\mathrm{l}=1}^{\mathrm{N}} d^{\mathrm{n}}_{\mathrm{jl}} \right) y_{\mathrm{i}} + k^{-\mathrm{n}}_{\mathrm{ji}} d^{\mathrm{n}}_{\mathrm{ji}} \right] \tag{A9}$$

$$\dot{d}^{\mathrm{i}}_{\mathrm{jn}} = k^{\mathrm{i}}_{\mathrm{jn}} \left(d_{\mathrm{i}} - \sum_{\mathrm{l}=1}^{\mathrm{N}} d^{\mathrm{i}}_{\mathrm{jl}} \right) y_{\mathrm{n}} - k^{-\mathrm{i}}_{\mathrm{jn}} d^{\mathrm{i}}_{\mathrm{jn}} \tag{A10}$$

$$\dot{m}_{\mathrm{i}} = d_{\mathrm{i}}\alpha_{\mathrm{i}}(\mathbf{D}_{\mathrm{i}}) - \gamma_{\mathrm{m,i}} m_{\mathrm{i}}. \tag{A11}$$

Among the reactions in Eqs. A8–A11, dimerization and protein binding/dissociation reactions are usually fast, while transcription, translation, and degradation are slow. This is not to say that there are only two timescales present in the system. On the contrary, gene networks can possess a diverse spectrum of timescales. However, these timescales can usually be partitioned into two classes—those that occur on fast timescales, and those that are slow in comparison. When such a partitioning occurs, it becomes possible to characterize the ratio of the characteristic time constants of fast and slow reactions by the small parameter ϵ, and introduce scaled kinetic constants for the slow reactions, $\tilde{\gamma}_{\mathrm{p,i}} = \varepsilon^{-1}\gamma_{\mathrm{p,i}}$, $\tilde{\alpha}_{\mathrm{i}} = \varepsilon^{-1}\alpha_{\mathrm{i}}$, $\tilde{\gamma}_{\mathrm{m,i}} = \varepsilon^{-1}\gamma_{\mathrm{m,i}}$, $\tilde{\sigma}_{\mathrm{i}} = \varepsilon^{-1}\sigma_{\mathrm{i}}$, and $\tilde{p}_{\mathrm{ij}} = \varepsilon^{-1}p_{\mathrm{ij}}$. In the spirit of multiple timescale analysis we introduce the fast and slow times t and $T = \epsilon t$, respectively. We assume that all concentrations are functions of these two independent variables and expand them in a power series in the small parameter, ϵ,

$$z = z^{(0)} + \epsilon z^{(1)} + \epsilon^2 z^{(2)} + \ldots, \tag{A12}$$

where $z = z(t, T)$ stands for variables x_{i}, y_{i}, $d^{\mathrm{i}}_{\mathrm{j}0}$, m_{i}, and $d^{\mathrm{i}}_{\mathrm{jn}}$. We replace the time derivatives in Eqs. A8–A11 by $\partial/\partial t + \epsilon\partial/\partial T$. Then, collecting terms of equal power of ϵ we obtain:

$$O(\epsilon^0)$$

$$\partial_{\mathrm{t}} x_{\mathrm{i}}^{(0)} = -2\kappa_{\mathrm{i}} [x_{\mathrm{i}}^{(0)}]^2 + 2\kappa_{-\mathrm{i}} y_{\mathrm{i}}^{(0)} \tag{A13}$$

$$\partial_{\mathrm{t}} y_{\mathrm{i}}^{(0)} = \kappa_{\mathrm{i}} [x_{\mathrm{i}}^{(0)}]^2 - \kappa_{-\mathrm{i}} y_{\mathrm{i}}^{(0)} + \sum_{\mathrm{n}=1}^{\mathrm{N}} \sum_{\mathrm{j}=1}^{\mathrm{M_n}} \left[-k^{\mathrm{n}}_{\mathrm{ji}} \left(d_{\mathrm{n}} - \sum_{\mathrm{l}=1}^{\mathrm{N}} d^{\mathrm{n}(0)}_{\mathrm{jl}} \right) y_{\mathrm{i}}^{(0)} + \ldots\ldots + k^{-\mathrm{n}}_{\mathrm{ji}} d^{\mathrm{n}(0)}_{\mathrm{ji}} \right] \tag{A14}$$

$$\partial_{\mathrm{t}} d^{\mathrm{i}(0)}_{\mathrm{jn}} = k^{\mathrm{i}}_{\mathrm{jn}} \left(d_{\mathrm{i}} - \sum_{\mathrm{l}=1}^{\mathrm{N}} d^{\mathrm{i}(0)}_{\mathrm{jl}} \right) y_{\mathrm{n}}^{(0)} - k^{-\mathrm{i}}_{\mathrm{jn}} d^{\mathrm{i}(0)}_{\mathrm{jn}} \tag{A15}$$

$$\partial_{\mathrm{t}} m_{\mathrm{i}}^{(0)} = 0 \tag{A16}$$

$$O(\epsilon^1)$$

$$\partial_{\mathrm{t}} x_{\mathrm{i}}^{(1)} + 4\kappa_{\mathrm{i}} x_{\mathrm{i}}^{(1)} x_{\mathrm{i}}^{(0)} - 2\kappa_{-\mathrm{i}} y_{\mathrm{i}}^{(1)} = -\partial_{\mathrm{T}} x_{\mathrm{i}}^{(0)} - \tilde{\gamma}_{\mathrm{p,i}} x_{\mathrm{i}}^{(0)} + \tilde{\sigma}_{\mathrm{i}} n_{\mathrm{i}} m_{\mathrm{i}}^{(0)} - x_{\mathrm{i}}^{(0)} \sum_{\mathrm{j}=1}^{\mathrm{N}} \tilde{p}_{\mathrm{ij}} x_{\mathrm{j}}^{(0)} \tag{A17}$$

$$\partial_{\mathrm{t}} y_{\mathrm{i}}^{(1)} - 2\kappa_{\mathrm{i}} x_{\mathrm{i}}^{(0)} x_{\mathrm{i}}^{(1)} + \kappa_{-\mathrm{i}} y_{\mathrm{i}}^{(1)} - \ldots \ldots - \sum_{\mathrm{n}=1}^{\mathrm{N}} \sum_{\mathrm{j}=1}^{\mathrm{M_n}} \left[k^{\mathrm{n}}_{\mathrm{ji}} \sum_{\mathrm{l}=1}^{\mathrm{N}} (d^{\mathrm{n}(0)}_{\mathrm{jl}} y_{\mathrm{i}}^{(1)} + d^{\mathrm{n}(1)}_{\mathrm{jl}} y_{\mathrm{i}}^{(0)}) + k^{-\mathrm{n}}_{\mathrm{ji}} d^{\mathrm{n}(1)}_{\mathrm{ji}} \right] = -\partial_{\mathrm{T}} y_{\mathrm{i}}^{(0)} \tag{A18}$$

$$\partial_{\mathrm{t}} d^{\mathrm{i}(1)}_{\mathrm{jn}} + k^{\mathrm{i}}_{\mathrm{jn}} \sum_{\mathrm{l}=1}^{\mathrm{N}} (d^{\mathrm{i}(0)}_{\mathrm{jl}} y_{\mathrm{n}}^{(1)} + d^{\mathrm{i}(1)}_{\mathrm{jl}} y_{\mathrm{n}}^{(0)}) + k^{-\mathrm{i}}_{\mathrm{jn}} d^{\mathrm{i}(1)}_{\mathrm{jn}} = -\partial_{\mathrm{T}} d^{\mathrm{i}(0)}_{\mathrm{jn}} \tag{A19}$$

$$\partial_{\mathrm{t}} m_{\mathrm{i}}^{(1)} = -\partial_{\mathrm{T}} m_{\mathrm{i}}^{(0)} + d_{\mathrm{i}} \tilde{\alpha}_{\mathrm{i}}(\mathbf{D}_{\mathrm{i}}^{(0)}) - \tilde{\gamma}_{\mathrm{m,i}} m_{\mathrm{i}}^{(0)}, \tag{A20}$$

etc.

We assume that for large times, $t \gg 1$, the solution of Eqs. A13–A16 reaches local equilibrium found from the set of algebraic equations

$$y_{\mathrm{i}}^{(0)} = H_{\mathrm{i}} [x_{\mathrm{i}}^{(0)}]^2 \tag{A21}$$

$$d^{\mathrm{i}(0)}_{\mathrm{jn}} = G^{\mathrm{i}}_{\mathrm{jn}} \left(d_{\mathrm{i}} - \sum_{\mathrm{l}=1}^{\mathrm{N}} d^{\mathrm{i}(0)}_{\mathrm{jl}} \right) y_{\mathrm{n}}^{(0)}, \tag{A22}$$

where $H_{\mathrm{i}} = \kappa_{\mathrm{i}}/\kappa_{-\mathrm{i}}$ and $G^{\mathrm{i}}_{\mathrm{jn}} = k^{\mathrm{i}}_{\mathrm{jn}}/k^{\mathrm{i}}_{-\mathrm{jn}}$.

To avoid secular growth of the first-order corrections, the right-hand side of the system, Eqs. A17–A20, must be orthogonal to the nullspace of the corresponding adjoint linear operator. At large time t the time derivatives in the left-hand side of Eqs. A17–A20 can be discarded, and the adjoint linear operator becomes a matrix. Its nullspace contains $2N$ eigenvectors,

$$\{x_i = 0,\ y_i = 0,\ d^i_{jn} = 0,\ m_i = \delta_{ii'}\},$$
$$\{x_i = \delta_{ii'},\ y_i = 2\delta_{ii'},\ d^i_{jn} = 2\delta_{ii'},\ m_i = 0\}, \tag{A23}$$

where δ_{ij} is the Krönecker delta function and $i' = 1 \ldots N$. The orthogonality conditions yield the equations

$$\partial_{\mathrm{T}} \left[x_{\mathrm{i}} + 2H_{\mathrm{i}} x_{\mathrm{i}}^2 + 2 \sum_{\mathrm{j}=1}^{\mathrm{M_i}} \sum_{\mathrm{n}=1}^{\mathrm{N}} d^{\mathrm{n}}_{\mathrm{ji}} \right] = \tilde{\sigma}_{\mathrm{i}} n_{\mathrm{i}} m_{\mathrm{i}} - \tilde{\gamma}_{\mathrm{p,i}} x_{\mathrm{i}} - \ldots \ldots - x_{\mathrm{i}} \sum_{\mathrm{j}=1}^{\mathrm{N}} \tilde{p}_{\mathrm{ij}} x_{\mathrm{j}}, \tag{A24}$$

$$\partial_{\mathrm{T}} m_{\mathrm{i}} = d_{\mathrm{i}} \tilde{\alpha}_{\mathrm{i}}(\mathbf{D}_{\mathrm{i}}) - \tilde{\gamma}_{\mathrm{m,i}} m_{\mathrm{i}}, \tag{A25}$$

where we have dropped the superscript (0) from the zero order variables.

The concentrations $d^{\mathrm{i}}_{\mathrm{jn}}$ for each binding site j have to be found from the algebraic system, Eqs. A21 and A22. These concentrations can be found explicitly,

$$d^{\mathrm{i}}_{\mathrm{jn}} = \frac{d_{\mathrm{i}} G^{\mathrm{i}}_{\mathrm{jn}} H_{\mathrm{n}} x_{\mathrm{n}}^2}{1 + \sum_{\mathrm{l}=1}^{\mathrm{N}} G^{\mathrm{i}}_{\mathrm{jl}} H_{\mathrm{l}} x_{\mathrm{l}}^2}. \tag{A26}$$

Next, we must find an expression for $\tilde{\alpha}_{\mathrm{i}}(\mathbf{D}_{\mathrm{i}})$. If we assume noncooperativity, then the probabilities of being in each state of the promoter are completely independent of one another. Therefore, we can rewrite Eq. A2 as

$$\tilde{\alpha}_{\mathrm{i}}(\mathbf{D}_{\mathrm{i}}) = \sum_{\mathbf{s}_{\mathrm{i}}} \tilde{\alpha}_{\mathrm{i}}(\mathbf{s}_{\mathrm{i}}) P_{\mathrm{i}}(\mathbf{s}_{\mathrm{i}}) = \sum_{\mathbf{s}_{\mathrm{i}}} \left\{ \tilde{\alpha}_{\mathrm{i}}(\mathbf{s}_{\mathrm{i}}) d_{\mathrm{i}}^{-\mathrm{M_i}} \prod_{\mathrm{j}=1}^{\mathrm{M_i}} d^{\mathrm{i}}_{\mathrm{j}\nu_{\mathrm{j}}} \right\}, \tag{A27}$$

where $P_{\mathrm{i}}(\mathbf{s}_{\mathrm{i}})$ is the probability that the i^{th} promoter is in the state $\boldsymbol{s}_{\mathrm{i}}$. Next we note that from Eqs. A1 and A26 we can derive the relation

$$d^{\mathrm{i}}_{\mathrm{j}0} = \frac{d_{\mathrm{i}}}{1 + \sum_{\mathrm{l}=1}^{\mathrm{N}} G^{\mathrm{i}}_{\mathrm{jl}} H_{\mathrm{l}} x_{\mathrm{l}}^2}. \tag{A28}$$

Furthermore, if we define $G^{\mathrm{i}}_{\mathrm{j}0}H_0x_0^2 = 1$, then we can write

$$d^{\mathrm{i}}_{\mathrm{jn}} = \frac{d_{\mathrm{i}}G^{\mathrm{i}}_{\mathrm{jn}}H_{\mathrm{n}}x_{\mathrm{n}}^2}{\sum_{\mathrm{l}=0}^{\mathrm{N}}G^{\mathrm{i}}_{\mathrm{jl}}H_{\mathrm{l}}x_{\mathrm{l}}^2}. \tag{A29}$$

Note that Eq. A29 is equivalent to Eq. A26, but only Eq. A29 is valid for $n = 0$. Therefore

$$\tilde{\alpha}_{\mathrm{i}}(\mathbf{D}_{\mathrm{i}}) = \sum_{\mathbf{s}_{\mathrm{i}}}\left\{\tilde{\alpha}(\mathbf{s}_{\mathrm{i}})\prod_{\mathrm{j}=1}^{\mathrm{M_i}}\frac{G^{\mathrm{i}}_{\mathrm{j}\nu_{\mathrm{j}}}H_{\nu_{\mathrm{j}}}x_{\nu_{\mathrm{j}}}^2}{\sum_{\mathrm{l}=0}^{\mathrm{N}}G^{\mathrm{i}}_{\mathrm{jl}}H_{\mathrm{l}}x_{\mathrm{l}}^2}\right\}. \tag{A30}$$

Plugging Eqs. A29 and A30 into Eqs. A24 and A25, we arrive at the set of $2N$ equations with the prefactors:

$$\left(1 + 4H_{\mathrm{i}}x_{\mathrm{i}} + 4H_{\mathrm{i}}x_{\mathrm{i}}\sum_{\mathrm{j}=1}^{\mathrm{M_i}}\sum_{\mathrm{n}=1}^{\mathrm{N}}\frac{d_{\mathrm{n}}G^{\mathrm{n}}_{\mathrm{ji}}}{\sum_{\mathrm{l}=0}^{\mathrm{N}}G^{\mathrm{n}}_{\mathrm{jl}}H_{\mathrm{l}}x_{\mathrm{l}}^2}\right)\partial_{\mathrm{T}}x_{\mathrm{i}} - \ldots$$
$$\ldots - 4H_{\mathrm{i}}x_{\mathrm{i}}^2\sum_{\mathrm{j}=1}^{\mathrm{M_i}}\sum_{\mathrm{n}=1}^{\mathrm{N}}\sum_{\mathrm{q}=1}^{\mathrm{N}}\frac{d_{\mathrm{n}}G^{\mathrm{n}}_{\mathrm{ji}}G^{\mathrm{n}}_{\mathrm{jq}}H_{\mathrm{q}}x_{\mathrm{q}}\partial_{\mathrm{T}}x_{\mathrm{q}}}{\left(\sum_{\mathrm{l}=0}^{N}G^{\mathrm{n}}_{\mathrm{jl}}H_{\mathrm{l}}x_{\mathrm{l}}^2\right)^2}\cdots$$
$$\ldots = \tilde{\sigma}_{\mathrm{i}}n_{\mathrm{i}}m_{\mathrm{i}} - \tilde{\gamma}_{\mathrm{p,i}}x_{\mathrm{i}} - x_{\mathrm{i}}\sum_{\mathrm{j}=1}^{\mathrm{N}}\tilde{p}_{\mathrm{ij}}x_{\mathrm{j}} \tag{A31}$$

$$\partial_{\mathrm{T}}m_{\mathrm{i}} = d_{\mathrm{i}}\sum_{\mathbf{s}_{\mathrm{i}}}\left\{\tilde{\alpha}_{\mathrm{i}}(\mathbf{s}_{\mathrm{i}})\prod_{\mathrm{j}=1}^{\mathrm{M_i}}\frac{G^{\mathrm{i}}_{\mathrm{j}\nu_{\mathrm{j}}}H_{\nu_{\mathrm{j}}}x_{\nu_{\mathrm{j}}}^2}{\sum_{\mathrm{l}=0}^{\mathrm{N}}G^{\mathrm{n}}_{\mathrm{jl}}H_{\mathrm{l}}x_{\mathrm{l}}^2}\right\} - \tilde{\gamma}_{\mathrm{m,i}}m_{\mathrm{i}}. \tag{A32}$$

Although the above derivation is applicable to a large class of gene regulatory networks, it is by no means comprehensive. There are many systems to which Eqs. A31 and A32 do not apply. For instance, some regulatory proteins, like *Lac*I, bind to promoter sites as tetramers, and not dimers (31,32). Furthermore, phenomena such as cooperative binding to promoter sites (33,34), enzymatic degradation (35,36), the formation of multimeric and hybrid protein complexes (37), and cellular growth and division (38) are not included in the model. For such cases, it is easy to rederive the equations to suit the particular needs of the model.

For an example of how to use Eqs. A31 and A32, let us once again derive the reduced equations for the repressilator, Eqs. 30 and 31. First there are $N = 3$ genes, each with $M_{\mathrm{i}} = 1$ promoter sites and the same concentration $d_{\mathrm{i}} = d$. Each protein has the same affinity to its dimer, so $H_{\mathrm{i}} = c_{\mathrm{p}}$, and there are no protein-protein degradation reactions ($p_{\mathrm{ij}} = 0$). Each dimer acts as a repressor for one of the other genes, in a ring fashion. The equilibrium constant, c_{d}, of the dimers to their associated promoter sites is the same for each, and since $M_{\mathrm{i}} = 1$ for each gene we can write $G^{\mathrm{n}}_{\mathrm{ji}} = G_{\mathrm{in}}$, where

$$\mathbf{G} = \begin{bmatrix} 0 & c_{\mathrm{p}} & 0 \\ 0 & 0 & c_{\mathrm{p}} \\ c_{\mathrm{p}} & 0 & 0 \end{bmatrix}. \tag{A33}$$

Next, we must assign values to the transcriptional rates, $\tilde{\alpha}_{\mathrm{i}}(\mathbf{s}_{\mathrm{i}})$. Since each gene has only one promoter site, and each promoter site can bind to only one dimer, the state vector turns out to be a scalar that can take on only two values, either zero (meaning no dimer is bound) or an integer $n \in \{1, 2, 3\}$ representing the index of the allowed repressor dimer. We are assuming complete repression, so that $\tilde{\alpha}$ has a nonzero value only when it is free. Therefore we can write $\tilde{\alpha}_{\mathrm{i}}(s_{\mathrm{i}}) = \alpha\delta_{s_{\mathrm{i}},0}$. Furthermore, we set $\tilde{\sigma}_{\mathrm{i}} = \sigma$, $n_{\mathrm{i}} = 1$, $\tilde{\gamma}_{\mathrm{p,i}} = \gamma_{\mathrm{p}}$, and $\tilde{\gamma}_{\mathrm{m,i}} = \gamma_{\mathrm{m}}$.

When we plug the above definitions into Eqs. A31 and A32 we arrive at the correct reduced equations for the repressilator. For instance, for x_1 and m_1 we get

$$\left\{1 + 4c_{\mathrm{d}}x_1 + \frac{4n_{\mathrm{c}}c_{\mathrm{d}}c_{\mathrm{p}}x_1}{\left(1 + c_{\mathrm{d}}c_{\mathrm{p}}x_1^2\right)^2}\right\}\dot{x}_1 = \sigma m_1 - \gamma_{\mathrm{p}}x_1, \tag{A34}$$

$$\dot{m}_1 = \frac{d\alpha}{1 + c_{\mathrm{d}}c_{\mathrm{p}}x_3^2} - \gamma_{\mathrm{m}}m_1. \tag{A35}$$

Analogous equations can be obtained for the other variables. When these equations are rescaled to dimensionless variables, they coincide with Eqs. 30 and 31.

The authors thank Tim Elston for useful discussions and creative ideas leading to the inception of this work.

This work was supported by the National Institutes of Health grant No. GM69811-01.

REFERENCES

1. Tyson, J. J., K. C. Chen, and B. Novak. 2003. Sniffers, buzzers, toggles and blinkers: dynamics of regulatory and signaling pathways in the cell. *Curr. Opin. Cell Biol.* 15:221–231.
2. Gillespie, D. T. 1977. Exact stochastic simulation of coupled chemical reactions. *J. Phys. Chem.* 81:2340–2361.
3. Rao, C. V., and A. P. Arkin. 2003. Stochastic chemical kinetics and the quasi-steady-state assumption: application to the Gillespie algorithm. *J. Chem. Phys.* 118:4999–5010.
4. Hasty, J., F. Isaacs, M. Dolnik, D. McMillen, and J. J. Collins. 2001. Designer gene networks: towards fundamental cellular control. *Chaos.* 11:207–220.
5. Isaacs, F. J., J. Hasty, C. R. Cantor, and J. Collins. 2003. Prediction and measurement of an autoregulatory genetic model. *Proc. Natl. Acad. Sci. USA.* 100:7714–7719.
6. Kepler, T. B., and T. C. Elston. 2001. Stochasticity in transcriptional regulation: origins, consequences and mathematical representations. *Biophys. J.* 81:3116–3136.
7. Tzafriri, A. R., and E. R. Edelman. 2004. The total quasi-steady-state approximation is valid for reversible enzyme kinetics. *J. Theor. Biol.* 226:303–313.
8. Elowitz, M. B., and S. Leibler. 2000. A synthetic oscillatory network of transcriptional regulators. *Nature.* 403:335–338.
9. Hasty, J., M. Dolnik, V. Rottschäfer, and J. J. Collins. 2002. Synthetic gene network for entraining and amplifying cellular oscillations. *Phys. Rev. Lett.* 88:148101.
10. Gonze, D., J. Leloup, and A. Goldbeter. 2000. Theoretical models for circadian rhythms in *Neurospora* and *Drosophila*. *Life Sci.* 323:57–67.
11. Fung, E., W. W. Wong, J. K. Suen, T. Butler, S. Lee, and J. C. Liao. 2005. A synthetic gene-metabolic oscillator. *Nature.* 435:118–122.
12. Bundschuh, R., F. Hayot, and C. Jayaprakash. 2003. Fluctuations and slow variables in genetic networks. *Biophys. J.* 84:1606–1615.
13. Arkin, A., J. Ross, and H. H. McAdams. 1998. Stochastic kinetic analysis of developmental pathway bifurcation in phage λ-infected *Escherichia coli* cells. *Genetics.* 149:1633–1648.
14. Ozbudak, E. M., M. Thattai, H. N. Lim, B. I. Shraiman, and A. van Oudenaarden. 2004. Multistability in the lactose utilization network of *Escherichia coli*. *Nature.* 427:737–740.
15. Pirone, J. R., and T. C. Elston. 2004. Fluctuations in transcription factor binding can explain the graded and binary responses observed in inducible gene expression. *J. Theor. Biol.* 226:111–121.
16. Mallet-Paret, J., and H. L. Smith. 1990. The Poincaré-Bendixson theorem for monotone cyclic feedback systems. *J. Dyn. Diff. Eqs.* 2:367–421.
17. Gardner, T. S., C. R. Cantor, and J. J. Collins. 2000. Construction of a genetic toggle switch in *Escherichia coli*. *Nature.* 403:339–342.
18. Bray, D. 1995. Protein molecules as computational elements in living cells. *Nature.* 376:307.
19. Weiss, R., and T. F. Knight. 2000. Engineered communications for microbial robotics. DNA6: Sixth International Meeting on DNA Based Computers (Leiden, The Netherlands).

20. Ptashne, M. 2004. A Genetic Switch: Phage Lambda Revisited, 3rd Ed. CSHL Press, Cold Spring Harbor, New York.

21. Michaelis, L., and M. L. Menten. 1913. The kinetics of the inversion effect. *Biochem. Z.* 49:333–369.

22. Briggs, G. E., and J. B. S. Haldane. 1925. A note on the kinetics of enzyme action. *Biochem. J.* 19:339.

23. Segel, L. A. 1988. On the validity of the steady state assumption of enzyme kinetics. *Bull. Math. Biol.* 50:579–593.

24. Stoleriu, I., F. A. Davidson, and J. L. Liu. 2004. Quasi-steady state assumptions for non-isolated enzyme-catalyzed reactions. *J. Math. Biol.* 48:82–104.

25. Wang, X., N. Hao, H. G. Dohlman, and T. C. Elston. 2006. Bistability, stochasticity, and oscillations in the mitogen-activated protein kinase cascade. *Biophys. J.* 90:1961–1978.

26. Sprinzak, D., and M. B. Elowitz. 2005. Reconstruction of genetic circuits. *Nature.* 438:443–448.

27. Acar, M., A. Becskei, and A. van Oudenaarden. 2005. Enhancement of cellular memory by reducing stochastic transitions. *Nature.* 435:228–232.

28. Raser, J. M., and E. K. O'Shea. 2005. Noise in gene expression: origins, consequences, and control. *Science.* 309:2010–2013.

29. Simpson, M. L., C. D. Cox, and G. S. Sayler. 2003. Frequency domain analysis of noise in autoregulated gene circuits. *Proc. Natl. Acad. Sci. USA.* 100:4551–4556.

30. Jordan, D. W., and P. Smith. 1987. Nonlinear Ordinary Differential Equations, 2nd Ed. Oxford University Press, Oxford, UK.

31. Hsieh, M., and M. Brenowitz. 1997. Comparison of the DNA association kinetics of the Lac repressor tetramer, its dimeric mutant *LacI*^{adi}, and the native dimeric Gal repressor. *J. Biol. Chem.* 272: 22092–22096.

32. Rosario, C. J., and R. A. Bender. 2005. Importance of tetramer formation by the nitrogen assimilation control protein for strong repression of glutamate dehydrogenase formation in *Klebsiella pneumoniae*. *J. Bacteriol.* 187:8291–8299.

33. Dodd, I. B., K. E. Shearwin, A. J. Perkins, T. Burr, A. Hochschild, and J. B. Egan. 2004. Cooperativity in long-range gene regulation by the λ CI repressor. *Genes Dev.* 18:344–354.

34. Ptashne, M., and A. Gann. 2002. Genes and Signals. CSHL Press, Cold Spring Harbor, New York.

35. Kim, Y., R. E. Burton, B. M. Burton, R. T. Sauer, and T. A. Baker. 2000. Dynamics of substrate denaturation and translocation be the ClpXP degradation machine. *Mol. Cell.* 5:639–648.

36. Siddiqui, S. M., R. T. Sauer, and T. Baker. 2004. Role of the processing pore of the ClpX AAA+ ATPase in the recognition and engagement of specific protein substrates. *Genes Dev.* 18:369–374.

37. Ortega, J., H. S. Lee, M. R. Maurizi, and A. C. Steven. 2004. ClpA and ClpX ATPases bind simultaneously to opposite ends of ClpP peptidase to form active hybrid complexes. *J. Struct. Biol.* 146: 217–226.

38. Rosenfeld, N., J. W. Young, U. Alon, P. S. Swain, and M. B. Elowitz. 2005. Gene regulation at the single-cell level. *Science.* 307: 1962–1965.